Microsyst Technol (2006) 12: 796–802
DOI 10.1007/s00542-006-0168-1

TECHNICAL PAPER

J. C. Chiou · Y. J. Lin

Modeling and verification of the double frequency effect using a MEMS device

Received: 13 September 2005 / Accepted: 13 December 2005 / Published online: 12 May 2006
© Springer-Verlag 2006

Abstract The derivation, verification, and implication of the nonlinear dynamic and frequency response of electrostatic actuator due to the double frequency effect (DFE) were reported in this study. In particular, an extra mode called half mode was observed and measured in various studies. However, a complete in-depth discussion of the effect was not reported in the past. In the present study, a second-order dynamical equation was adapted firstly to model the dynamic and frequency response of electrostatic actuator where typical harmonic input signal with a dc bias was used. Secondly, by solving the equation, complex waveform in dynamic response and an extra half mode in frequency response due to the double frequency effect can be observed and discussed. To verify the simulated result, an electrostatic driving device was fabricated using PolyMUMPS© process. Note that in frequency response, when dc bias is equal to the amplitude of ac signal, simulated and experimental results indicated that the amplitude of half mode was one-fourth of first mode.

1 Introduction

Microelectromechanical systems (MEMS) enable suspended microstructures to be moved precisely and integrated with microelectronic circuits monolithically on a chip to perform or provide analog tuning or digital switching of linear or angular motion (Mohamed et al. 2003). Various actuation mechanisms, such as thermal/bimetallic bimorph (Mohamed et al. 2003; Popa et al. 2003; Tuantranont and Bright 2002), electromagnetic (Chowdhury et al. 2000; Ji et al. 2000), piezoelectric (Park et al. 2001; Haddab et al. 2000), and electrostatic actuation (Hung and Senturia 1999; Mu et al. 2003), have been established and applied fundamentally in MEMS-based devices where mechanical actuation is required.

Of the existing actuating methods for micro-actuator, electrostatic actuation is thought to be the most popular method to achieve fast-response-time and simple electronics (Rosa et al. 1998). In addition, the characteristic of low power consumption in both resonant and quasi-static operation is prompt to use in different harmonic motion applications, such as projection display, confocal laser scanning microscope, dynamic focusing lens, diffraction grating scanner, and barcode reader. Recently, various electrostatic actuator designs, such as the parallel plate, laterally comb-drive and vertical comb-drive actuators, had been developed to achieve digital switching or raster scanning applications.

In designing the aforementioned MEMS devices, its corresponding dynamic characteristic such as frequency response is an important ingredient in the design flow. When a micro-actuator is driven by a harmonic electrical input signal, the frequency response is obtained by recording the vibration magnitude and the driving signal from lower to highly frequencies. However, upon the scanning frequencies are closed to the so-called half mode, a smaller magnitude than that of natural mode had been observed as the parts of experiments without exclusive discussions (Ries and Smith 1998; Lee et al. 2004; Fleischmann et al. 2004). Wilfinger et al. pointed out that the appearance of half mode is due to the fact that electrostatic force is square proportional to the input electrical signal (Wilfinger et al. 1968; Jin et al. 1995; Kiang et al. 1998; Lin and Fang 2003).

By surveying other existing actuating technologies, half mode was also observed. In magnetic levitation application, the magnetic force varies as the square of the current and varies inversely with the square of the gap between the electromagnetic and the reaction surface (Piyabongkarn et al. 2005). A piezoelectric actuator

J. C. Chiou · Y. J. Lin (✉)
Department of Electrical and Control Engineering,
National Chiao Tung University, Hsin-Chu, Taiwan, ROC
E-mail: chiou@cc.nctu.edu.tw
E-mail: yjlin@cn.nctu.edu.tw
Tel.: +886-3-5731881
Fax: +886-3-5715998

is used to excite a deformable array (Ries and Smith 1998), and the half mode is clear observed from its frequency response. In conclusion, the half mode is existed not only in electrostatic actuation but also in other actuation principle such as electromagnetic, thermo, and piezoelectric actuators.

In this investigation, the dynamic response of electrostatic actuator with harmonic loading is presented and used to verify the double frequency effect (DFE) induced half mode. An actual device fabricated with PolyMUMPS© process was measured and proof the notable peak of half mode. The time domain response was also measured and discussed the distortion of waveform between the input and output. A parameter, AR, was defined to estimate the amplitude ratio of the half mode to the first mode.

2 Fabricated device, modeling, and derivation

As shown in Fig. 1, an electrostatic actuating micro-resonator device was modeled and measured. The device is fabricated using the commercial available PolyMUMPS© process (Koester et al. 1994). The process consists of a nitride isolation layer, three polysilicon structural layers (Poly0–2), two phosphosilicon glass sacrificial layers (PSG1 and PSG2), and a gold metal layer (Au) for optical reflection and electronic connection. After dicing process, Hydroflouric (HF) acid is used to release the MEMS structures. The micro-resonator consists of a composite beam (Rotor) is accomplished by deposit a 0.5 μm thick Au film on the surface of the 1.5 μm thick polysilicon (Poly2) and fixed to an anchor structure. Based on the tensile and compress residual stress of Au and Poly2 layer, the composite beam is exhibited a curved up out of plane behavior. An external electrode (stator) was manufactured in the flank of rotor to construct an electrostatic actuator. Note that, the electrostatic force was dominated by fringe effect due to the malposition design between rotor and stator. Therefore, the variation of C is limited, and $\partial C/\partial z$ is approximated to a constant in a larger operation region, and the typical drawbacks in electrostatic actuation such as pull-in and hysteresis phenomenon in the parallel plate electrostatic actuator will not occur in the current design (Rosa et al. 2004).

The applied electrostatic force of the device can be expressed as

$$F_{\mathrm{E}} = \frac{1}{2}\frac{\partial C}{\partial z}V^2, \tag{1}$$

where C is the equivalent capacitor between the rotor and stator of electrostatic actuator, z is the displacement of rotor, and V is the applied electrical driving signal. When the actuator is driven in small signal and/or lateral motion comb-drive, the partial differential of capacitor with respect to displacement, $\partial C/\partial z$, can be assumed to be a constant.

By intuition, when a harmonic motion output is required, an ac electrical input signal, $f_{\mathrm{I1}} = 2\sin(\omega_{\mathrm{I1}}t)$, is always chosen, as illustrated in Fig. 2a. However, the square nonlinear relationship between the V and F_{E} makes the electrostatic force, $f_{\mathrm{O1}} = f_{\mathrm{I1}}^2 = 2 - 2\cos(\omega_{\mathrm{O1}}t)$, be always positive even when f_{I1} is negative. From the schematic illustration in Fig. 2a, this nonlinear and frequency distortion phenomenon of DFE can be clearly observed. Consequently, a modified input signal, $f_{\mathrm{I2}} = 1 + \sin(\omega_{\mathrm{I2}}\,t)$, comprising of an ac harmonic with a dc bias signals, was used to improve the frequency distortion due to the DFE, as shown in Fig. 2b. This modified electrostatic force, $f_{\mathrm{O2}} = f_{\mathrm{I2}}^2 = 1.5 + 2\sin(\omega_{\mathrm{I2}}t) - 0.5\cos(2\omega_{\mathrm{I2}}t)$, with equivalent frequency was also shown in Fig. 2b. Note that, the frequency distortion is improved, however, the distortion such as dead zone appeared in the applied electrostatic force.

The micro-resonator is assumed to have a standard second-order dynamic system and a modified harmonic signal similar to the f_{I2} is used as the electrical excitation signal. Therefore, the corresponding dynamic equation can be expressed as

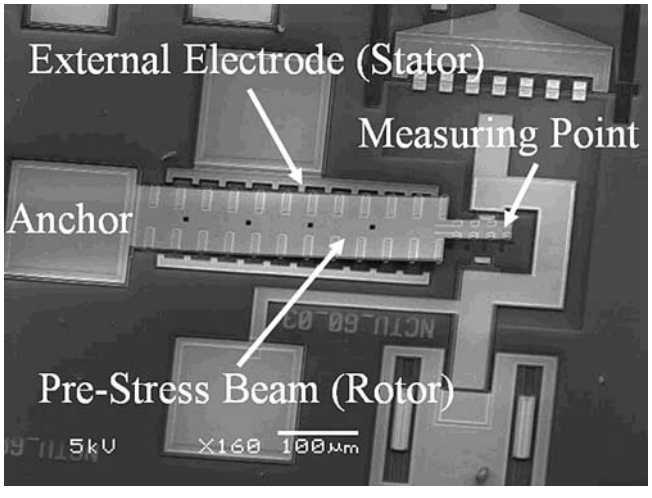

Fig. 1 Fabricated electrostatic actuating device

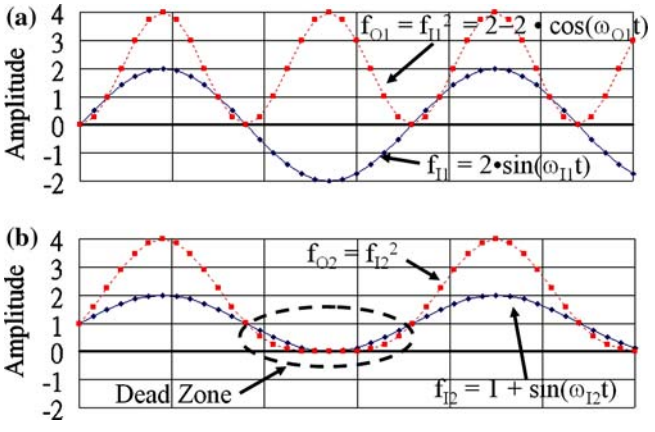

Fig. 2 Applied signals in electrostatic actuator

$$m\ddot{z} + c\dot{z} + kz = F_E = \frac{1}{2}\frac{\partial C}{\partial z}[a_0 + a_1\sin(\omega t)]^2 = \beta_p\left[a_0^2 + \frac{a_1^2}{2} + 2a_0a_1\sin(\omega t) - \frac{a_1^2}{2}\cos(2\omega t)\right] = f_0 + f_1(\omega t) - f_2(2\omega t), \quad (2)$$

where m is mass, c damping constant, k is equivalent spring constant, $\beta_p = (1/2)\ (\partial C/\partial z)$ is the capacitor constant of micro-resonator, and ω is the excitation frequency of electrical excitation signal. The coefficients a_0 and a_1 are denoted as the dc bias and the amplitude of ac signal, respectively, where $a_0 \geq a_1$ is assumed to ensure no negative input signal. Furthermore, $f_0 = \beta_p\left(a_0^2 + a_1^2/2\right)$ denotes as constant mechanical excitation input, $f_1(\omega t) = \beta_p(2a_0a_1\sin(\omega t))$ and $f_2(2\omega t) = \beta_p\left(\left(a_1^2/2\right)\cos(2\omega t)\right)$ denote as two different periodic mechanical excitation inputs. The solution of Eq. 2 can be derived and expressed as

$$z(\omega t) = z_H(\omega t) + z_{f_0}(\omega t) + z_{f_1}(\omega t) - z_{f_2}(2\omega t), \quad (3)$$

where $z_H(\omega\ t)$ is the homogeneous solution of Eq. 2, $z_{f_0}(\omega t)$ is the transient solution due to the f_0, $z_{f_1}(\omega t)$ is the periodic solution due to the f_1 $(\omega\ t)$, and $z_{f_2}(2\omega t)$ is the periodic solution due to f_2 $(2\omega\ t)$. Thus, the steady state solution of Eq. 3 can be obtained as follows:

$$\lim_{t\to\infty} z(\omega t) = z_0 + z_{f_1}(\omega t) - z_{f_2}(2\omega t) = z_0 + z_{ss}(\omega t), \quad (4)$$

where z_0 is the constant displacement, and z_{ss} $(\omega\ t)$ is the periodic steady state solution. Since the periodic steady state solution plays an important role in harmonic output, it can be further derived and rewritten as

$$z_{ss}(\omega t) = z_{f_1}(\omega t) - z_{f_2}(2\omega t) = Z_1\sin(\omega t - \phi_1) - Z_2\cos(2\omega t - \phi_2), \quad (5)$$

where

$$Z_1 = \beta_p\frac{K_1}{\sqrt{M_1^2 + D_1^2}} = \beta_p\frac{2a_0a_1/k}{\sqrt{(1-\beta^2)^2 + (2\zeta\beta)^2}}, \quad (6)$$

$$\phi_1 = \tan^{-1}\left(\frac{D_1}{M_1}\right) = \tan^{-1}\left(\frac{2\zeta\beta}{1-\beta^2}\right), \quad (7)$$

$$Z_2 = \beta_p\frac{K_2}{\sqrt{M_2^2 + D_2^2}} = \beta_p\frac{a_1^2/2k}{\sqrt{(1-4\beta^2)^2 + (4\zeta\beta)^2}}, \quad (8)$$

$$\phi_2 = \tan^{-1}\left(\frac{D_2}{M_2}\right) = \tan^{-1}\left(\frac{4\zeta\beta}{1-4\beta^2}\right), \quad (9)$$

$$\beta = \frac{\omega}{\omega_n}, \quad \omega_n = \sqrt{\frac{k}{m}}, \quad \zeta = \frac{c}{2\sqrt{km}}, \quad (10)$$

and Z_1 and Z_2 are the amplitude of the $z_{f_1}(\omega t)$ and $z_{f_2}(2\omega t)$, ϕ_1 and ϕ_2 are the phase shift with respect to $\omega\ t$ and $2\omega\ t$. *beta* is the ratio of the applied frequency to the natural frequency, ζ is the damping ratio and ω_n is the natural frequency of the system.

In Eq. 5, two resonant frequencies $\omega_n/2$ and ω_n are obtained due to the fact that $z_{ss}(\omega\ t)$ is a linear combination of $z_{f_1}(\omega t)$ and $z_{f_2}(2\omega t)$. In particular, when the input signal is adjacent to $\omega_n/2$, the response of $z_{ss}(\omega\ t)$ is dominated by $z_{f_2}(2\omega t)$. This characteristic can be observed as the input signal equals to $\omega_n/2$, Z_2 reaches its maximum amplitude as M_2 of Eq. 8 is closed to zero. As defined previously, this phenomenon is called the "half mode" of the system that is driven by V^2 term of Eq. 1. Likewise, as the input signal is closed to ω_n, namely the first mode, $z_{f_1}(\omega t)$ dominates the response of $z_{ss}(\omega\ t)$ which can be observed from Eq. 6 as M_1 is closed to zero.

Furthermore, we can further estimate the amplitude ratio of half and first mode, AR, by substituting individual frequency into $z_{f_1}(\omega t)$ and $z_{f_2}(2\omega t)$ that yields:

$$\mathrm{AR} = \frac{\left|z_{f_2}(2\omega t)\right|\big|_{\omega=\omega_n/2}}{\left|z_{f_1}(\omega t)\right|\big|_{\omega=\omega_n}} = \frac{Z_2|_{\beta=1/2}}{Z_1|_{\beta=1}} = \frac{a_1}{4a_0}. \quad (11)$$

When $a_0 = a_1$, AR = 1/4, the resonant amplitude of half mode is approximately one-fourth of first mode. Note that, as the scanning frequency is moving toward the resonant frequencies of $\omega_n/2$ and ω_n, the ratio of Z_2 to Z_1 is getting larger and larger, whereas as the scanning frequency is leaving the resonant frequencies of $\omega_n/2$ and ω_n, the ratio of Z_2 to Z_1 is getting smaller and smaller. The higher ratio of Z_2 to Z_1 causes the complex composite waveform. These phenomenons can be verified from the following simulation and measurement results.

3 Dynamic response simulation

In the present simulations, FEM simulation software, IntelliSuite®, was used to investigate the mode and extract the system parameters, $\omega_n = 2\pi \times 5{,}000$ rad/s, $a_0 = a_1 = 10$, $\zeta = 0.026$, $\beta_p = 0.0001$, $k = 0.1$. Figure 3 shows the $z_{ss}(\omega\ t)$ of micro-resonator driven in various frequencies. Note that, $z_{ss}(\omega\ t)$ is plotted inversely in order to match the measured data given in Sect. 5. As shown in Fig. 3a, when the frequency is lower than 1,500 Hz, a dead zone is occurred due to the actually mechanical excitation signal with distortion as shown in Fig. 2b. From Eqs. 5, 6, 7, 8, 9, and 10, we notice that when ω is lower than ω $_n/2$, Z_1, Z_2, ϕ_1 and ϕ_2 will increase as ω increases. On the other hand, if ω is higher than $\omega_n/2$, as ω increases, Z_1 and ϕ_1 will still increase but the Z_2 and ϕ_2 will start to decrease. These non-synchronous increased of amplitude and phase resulted in $z_{ss}(\omega\ t)$ to have two local minimum and maximum, as indicated in Fig. 3b–e. As ω is over 4,000 Hz, a well reciprocation output was obtained.

In order to obtain reliable reference data for the following experimental measurements, two reference frequencies at $\omega_n/2$ and ω_n are simulated. Figure 4 shows the simulation results of $z_{f_1}(\omega t)$, $z_{f_2}(2\omega t)$, and $z_{ss}(\omega\ t)$. The period of $z_{f_2}(2\omega t)$, defined as τ_2, is twice of

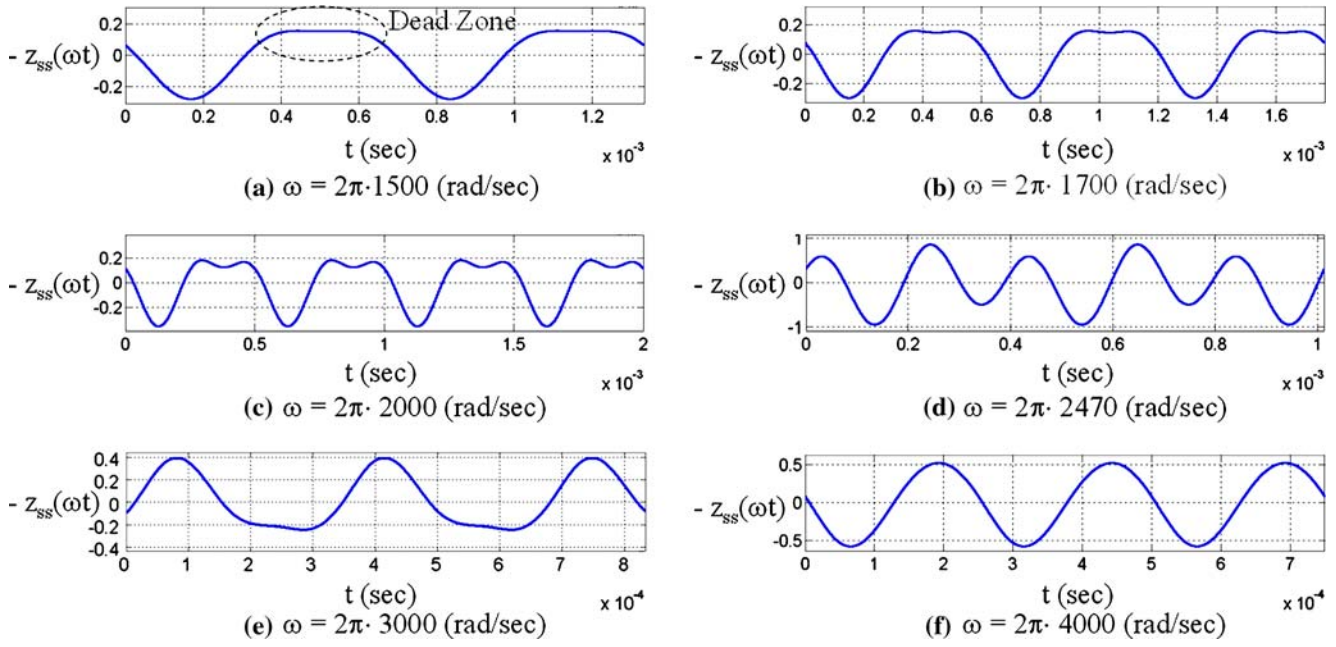

Fig. 3 The dynamic response of micro-resonator driven between 1.5 and 4 kHz

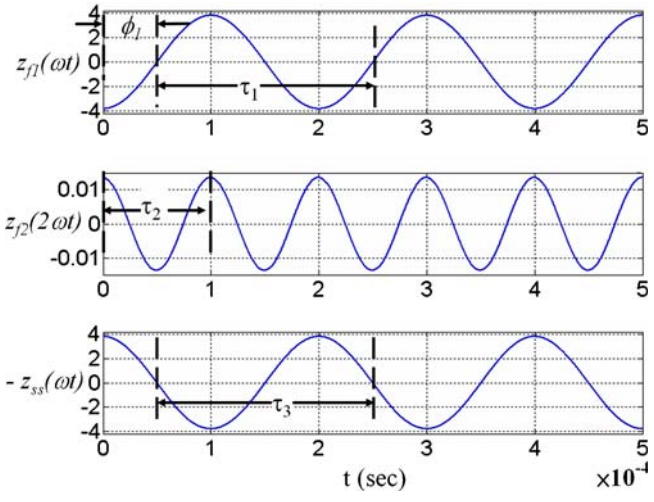

Fig. 4 The dynamic response of micro-resonator driven in $\omega = \omega_n$

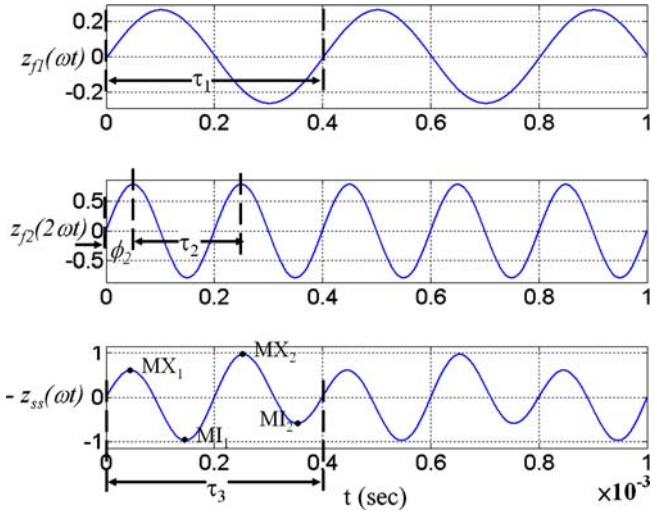

Fig. 5 The dynamic response of micro-resonator driven in $\omega = \omega_n/2$

the period of $z_{f_1}(\omega t)$, defined as τ_1, and $z_{ss}(\omega\ t)$, defined as τ_3. Since Z_1 is greatly larger than Z_2, thus the final amplitude and phase of $z_{ss}(\omega\ t)$ are dominated by $z_{f_1}(\omega t)$.

In Fig. 5, when ω is equal to $\omega_n/2$, τ_3 is tracking closely to τ_1. Nevertheless, since Z_1 and Z_2 are of the same magnitude, thus in complex waveform of τ_3, two local maximums, MX_1 and MX_2, and local minimums, MI_1 and MI_2, are induced.

4 Frequency response simulation

Figure 6 shows the frequency response simulation of the fabricated micro-resonator. Note that, the amplitude is denoted as the difference between MI_1 and MX_2. To match aforementioned analysis, a maximum peak of first mode is occurred at $\omega = \omega_n = 2\pi \times 5{,}000$ rad/s. A smaller peak due to half mode and the AR = 1/4 are observed in this simulation.

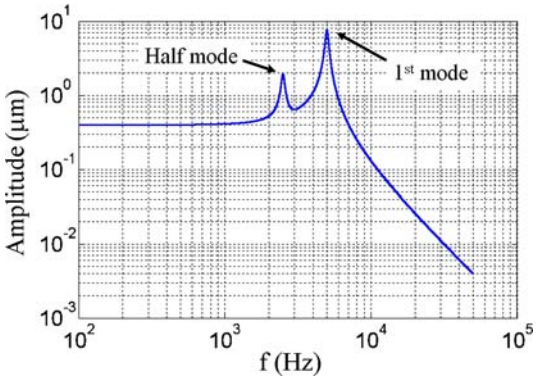

Fig. 6 The frequency response micro-resonator

5 Experiments and discussions

The released micro-resonator has been packaged using a DIP package for the purpose of measurements. A laser Doppler vibrometer (LDV) were used to measure the dynamic characteristics of micro-resonator and the measuring point was located close to the free end of micro-resonator, as shown in Fig. 1. The velocity of the free end of micro-resonator is measured with a LDV, and the displacement of the free end of micro-resonator is numerically integrated from the velocity.

5.1 Dynamic response measurement in harmonic loading

In the presented experiment, the applied electrical signal of the micro-resonator was biased by the sinusoidal wave with voltages peak to peak, 0–20 V (e.g., $a_0 = a_1 = 10$ V), and frequency range between 100 Hz and 4 kHz, as shown in Fig. 7a–f. When the bias signal is setting at the frequency range between 100 Hz and 1.5 kHz, the relative amplitude is fixed at 2.219 μm. Note that, the dead zone discussed in Sect. 3 was

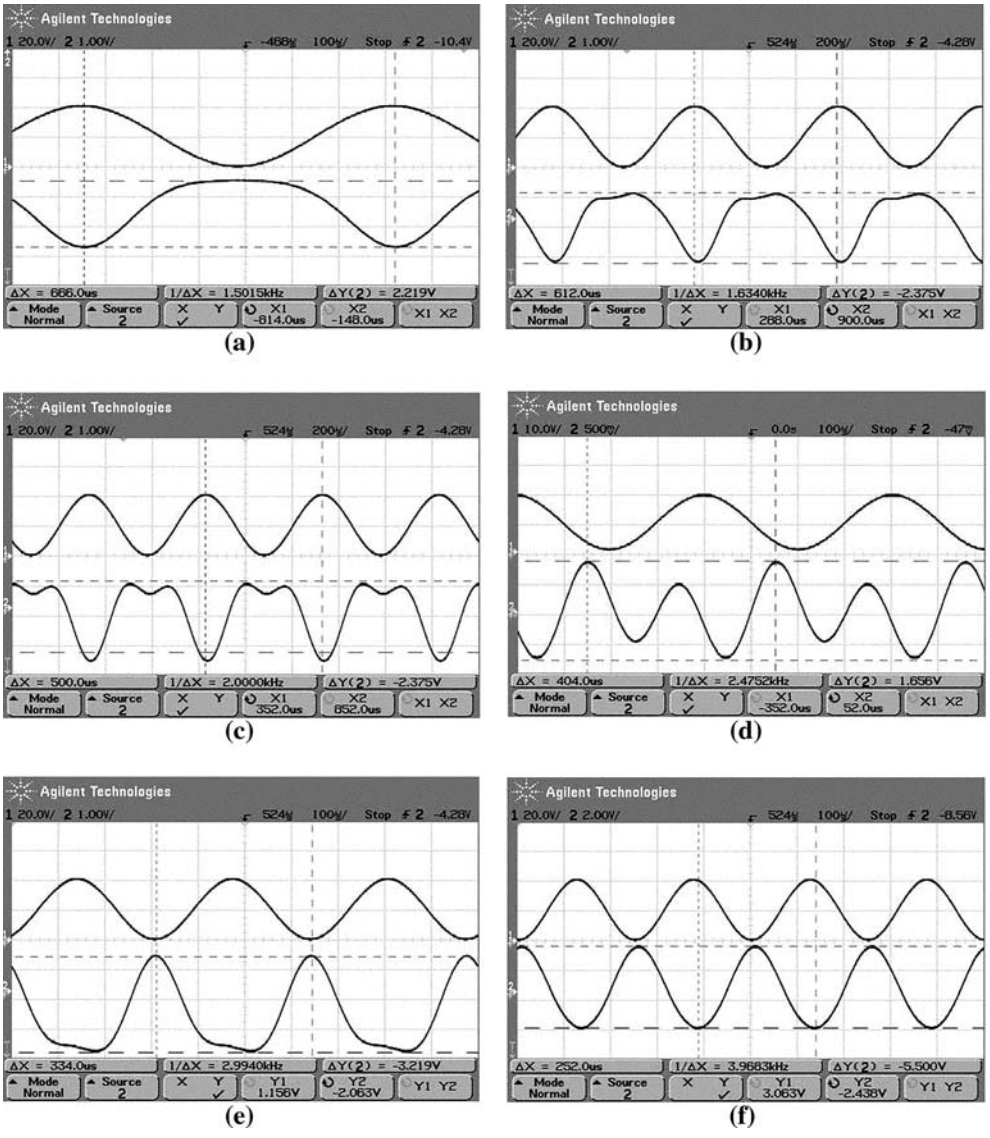

Fig. 7 The dynamic response of micro-resonator driven between 1.5 and 4 kHz (the *upper curve* is the input signal and the *lower curve* is the LDV output signal)

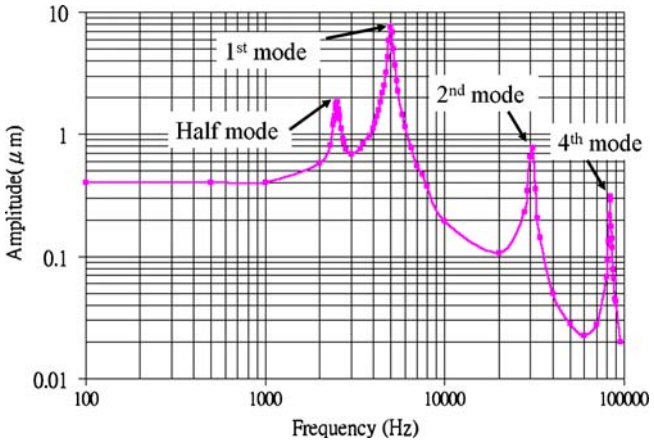

Fig. 8 The frequency response of micro-resonator

observed in Fig. 7a. Nevertheless, when the bias signal is over 1.5 kHz, the complex waveform due to DFE is observed, as shown in Fig. 7b–e. As soon as the frequency is over 3.9 kHz, the complex waveform is back to monotone waveform, as shown in Fig. 7f. The measured dynamic response of micro-resonator in Fig. 7 was match very well to the simulation results shown in Fig. 3.

5.2 Frequency response

As shown in Fig. 8, the frequency response of micro-resonator is obtained by using LDV. The applied electrical signal of micro-resonator was biased by the sinusoidal wave with voltages peak to peak, 0–20 V (e.g., $a_0 = a_1 = 10$ V), and frequency range from 100 Hz and 100 kHz. The half and first mode are measured at 2.5 and 5 kHz, which matched very well with the model analysis and simulations given in Sects. 2 and 4. From previous FEM simulations, second and fourth modes matched well with third and fourth peaks of Fig. 8 which are measured at 31 and 84.03 kHz, respectively. In the present experiment, AR = 1/4 is obtained due to the fact that $a_0 = a_1 = 10$ V.

Not that, the half modes of second and fourth mode were not observed in the measurement process due to the lower frequency sampling rate. Although not reported herein, we have observed the half mode of second mode in another resonator that was fabricated using CMOS–MEMS process.

6 Conclusion

This work describes the nonlinearly and distortion behavior in dynamic and frequency response of electrostatic actuator due to the DFE. A mathematical model of second-order dynamic system was used to express the dynamic and frequency response of electrostatic actuator. By using this mathematical model, the complex waveform in dynamic response and extra half mode in frequency response due to the DFE were illustrated, discussed, and simulated. To verify the simulated result, an electrostatic driving device was fabricated using PolyMUMPS© process. Note that, the simulation results of dynamic and frequency response were match very well with the measurement results. Furthermore, when the dc bias is equal to the amplitude of ac signal, as derived previously, the amplitude ratio of half mode was about one-fourth of first mode.

In the present study, the value of $\partial C/\partial z$ in Eq. 1 is assumed to be constant. However, in the other studies, this assumption is not conformed to the MEMS devices such as rotation mirror with parallel plate electrostatic actuation. Thus, in the case of non-constant $\partial C/\partial z$, Eq. 11 can no longer be used to predict AR. By fully understanding the present mathematical model and measurement results of electrostatic actuator, control algorithm will be developed in the future for novel applications.

Acknowledgments This work was supported in part by Ministry of Economic Affairs, Taiwan, ROC under Contract No. 92-EC-17-A-07-S1-0011, the National Science Council, Taiwan, ROC under Contract No. NSC 94-2218-E-009-031, NSC 94-2215-E-009-056 and by the Brian Research Center, University System of Taiwan, under Grant 92B-711.

References

Chowdhury S, Ahmadi M, Jullien GA, Miller WC (2000) A modular MEMS electromagnetic actuator for use in a hearing instrument. In: Proceedings of the 43rd IEEE midwest symposium on circuits and systems, vol 1, pp 240–243

Fleischmann T, Kubota K, Vaccaro PO, Wang TS, Saravanan S, Saito N (2004) Self-assembling GaAs mirror with electrostatic actuation using micro-origami. Physica E 24:78–81

Haddab Y, Chaillet N, Bourjault A (2000) A microgripper using smart piezoelectric actuators. In: Proceedings of IEEE international conference on intelligent robots and systems (IEEE/RSJ IROS), vol 1, pp 659–664

Hung ES, Senturia SD (1999) Extending the travel range of analog-tuned electrostatic actuators. J Microelectromech Syst 8(4):497–505

Ji CH, Kim YK, Choi BK (2000) Design and fabrication of electromagnetic micromirror with bulk silicon mirror plate and aluminum spring. In: Proceedings of IEEE/LEOS optical MEMS, pp 97–98

Jin Z, Wang Y, Xu Y, Ding C (1995) The properties of micromechanical resonator. In: International conference on solid-state and integrated circuit technology, pp 482–484

Kiang MH, Solgaard O, Lau KY, Muller RS (1998) Electrostatic combdrive-actuated micromirrors for laser-beam scanning and positioning. J Microelectromech Syst 7(1):27–37

Koester DA, Mahadevan R, Markus KW (1994) MUMPS introduction and design rules, MCNC MEMS Technology Applications Center

Lee D, Krishnamoorthy U, Yu K, Solgaard O (2004) Single-crystalline silicon micromirrors actuated by self-aligned vertical electrostatic combdrives with piston-motion and rotation capability. Sensors Actuat A 114:423–428

Lin HY, Fang WL (2003) A rib-reinforced micro torsional mirror driven by electrostatic torque generators. Sensors Actuat A 105:1–9

Mohamed A, Elsimar H, Ismail M (2003) Analysis, and optimization of a CMOS vertical thermal actuator. In: Proceedings of 2003 symposium on design, test, integration and packaging of MEMS/MOEMS, 5–7 May, pp 214–217

Mu XH, Kahrizi M, Landsberger L (2003) Design & fabrication of out-of-plane electrostatic actuators for optical application. In: Proceedings of IEEE Canadian conference on electrical and computer engineering (IEEE CCECE), vol 1, pp 133–136

Park JY, Yee YJ, Nam HJ, Bu JU (2001) Micromachined RF MEMS tunable capacitors using piezoelectric actuators. In: Proceedings of IEEE microwave symposium digest, vol 3, pp 2111–2114

Piyabongkarn D, Sun Y, Rajamani R, Sezen A, Nelson BJ (2005) Travel range extension of a MEMS electrostatic microactuator. IEEE Trans Contr Syst Technol 13(1):138–145

Popa DO, Byoung HK, Wen JT, Stephanou HE, Skidmore G, Geisberger A (2003) Dynamic modeling and input shaping of thermal bimorph MEMS actuators. In: Proceedings of IEEE international conference on robotics and automation (IEEE ICRA '03), vol 1, pp 1470–1475

Ries LL, Smith SW (1998) Phase aberration correction in two dimensions with an integrated deformable actuator/transducer. IEEE Trans Ultrason Ferroelectr Freq Contr 44(6):1366–1375

Rosa MA, Dimitrijev S, Harrison HB (1998) Enhanced electrostatic force generation capability of angled comb finger design used in electrostatic comb-drive actuators. Electron Lett 34(18):1787–1788

Rosa MA, Bruyker DD, Volkel AR, Peeters E, Dunec J (2004) A novel external electrode configuration for the electrostatic actuation of MEMS based devices. J Micromech Microeng 14:446–451

Tuantranont A, Bright VM (2002) Micromachined thermal multimorph actuators fabricated by multi-users MEMS process. In: Proceedings of IEEE international conference on industrial technology (IEEE ICIT '02), vol 2, pp 941–944

Wilfinger RJ, Bardell PH, Chhabra DS (1968) The resonistor: a frequency selective device utilizing the mechanical resonance of a silicon substrate. IBM J Res Dev 12:113–118